#252 — Dupl

#252
UR-459 (138-I & II)
FERMILAB-PUB-73-151-E PRL

CROSS SECTIONS AND CHARGED PARTICLE MULTIPLICITIES AT 102 and 405 GeV +

C. Bromberg, D. Chaney, D. Cohen*, T. Fertel†, P. Slattery and D. Underwood

University of Rochester

Rochester, N.Y. 14627

J.W. Chapman, J.W. Cooper, H. Grean, B.P. Roe, A.A. Seidl, and J. C. Vander Velde

University of Michigan

Ann Arbor, Mich. 48104

We have measured the total inelastic cross section (σ_{inel}) and charged-particle multiplicities obtained in pp collisions at 405 GeV. The data are from a preliminary 12,000 picture exposure of the 30-inch ANL/NAL liquid-hydrogen bubble chamber. We find $\sigma_{inel} = 32.8 \pm 1.0$ mb; the low moments of the multiplicity distribution for negative particles are: $\langle n_- \rangle = 3.50 \pm 0.07$, $D_- = 2.37 \pm 0.05$, $f_2^- = 2.1 \pm 0.2$, $f_3^- = 0.1 \pm 0.9$. We also present updated results at 102 GeV.

+Research supported by the U. S. Atomic Energy Commission. Computing funds at the University of Rochester are provided by the University.

*Present Address: Nevis Laboratories, Columbia University Irvington-on-Hudson, New York.

†A. P. Sloan Fellow.

In this letter we report our latest measurements of topological, elastic, and total cross sections in pp collisions at 102 and 405 GeV utilizing the 30-inch ANL/NAL liquid-hydrogen bubble chamber. The 102 GeV data are from a 31,000 picture exposure (about 128 events per mb of cross section), while the 405 GeV data are from a 12,000 picture exposure (about 65 events per mb of cross section). The present work supercedes a previous publication of preliminary results at 102 GeV based on a 5000 picture exposure.[1]

Both exposures were scanned twice for events produced by beam-like tracks; a third comparison scan was performed to adjudicate any inconsistencies in beam counts or event topologies found in the two previous independent scans of the film. The 405 GeV data and the initial 102 GeV exposure[1] were taken using 70 mm film, while the major fraction of the 102 GeV experiment was recorded using 35 mm film, with the chamber operating in a double-pulsing mode. All exposures were divided equally between the Michigan and Rochester Groups and were handled in a similar manner. Scanning at Michigan was performed using projectors having 40X magnification of the image from film to scanning table, while a 25X magnification was used at Rochester.

In Table I we present our measurements of the topological cross sections at 102 GeV Corrections to the charged-particle cross sections have been made for Dalitz decays of the π^0 mesons.[2] Results from the two scans indicated that the double-scan efficiency for visible two prongs (σ_2) was 99 ± 1%, while for higher-prong numbers it was essentially 100%. All apparent odd-pronged events (~0.2% of the total) were classified as belonging to even-pronged topologies of the next highest integer value. A small correction, corresponding to a shift in the multiplicity distribution of approximately 10% of that resulting from

the Dalitz-pair correction, was also applied to the data to take account of secondary interactions occurring within 0.5 cm of the main production vertex which might have gone unnoticed. Finally, the two-prong data were corrected for small-angle proton losses (short proton recoils which were not visible in the bubble chamber). The latter loss was determined by fitting the elastic scattering data to an exponential form:

$$\left.\frac{d\sigma}{dt}\right|_{t=0} e^{At + Bt^2} \qquad (1)$$

where t is the square of the four-momentum transfer from incident to outgoing proton. The fit was carried out using the unbiased data for $|t| > 0.05\ \mathrm{GeV}^2$, with the constraint that the cross section at t=0 be given by the lower limit provided by the optical theorem:[3]

$$\left.\frac{d\sigma}{dt}\right|_{t=0} = \frac{\sigma_T^2}{16\pi(\hbar c)^2} \qquad (2)$$

where for σ_T we used our measured value of the total cross-section (iterated with respect to the corrections required for $|t| < 0.05\ \mathrm{GeV}^2$).

Figure 1(a) displays the measured elastic differential cross-section at 102 GeV and the fit of Eq. (1) to the data. The best-fit parameters are given on the graph. The value of B is consistent with recent measurements reported at NAL.[3] The two-prong inelastic cross section was also corrected for slow-proton recoils assuming the same detection efficiency as a function of t as was found using the fit in Fig. 1.

The events appearing in the elastic cross-section data of Fig. 1 were obtained through kinematic fitting of all two-pronged events to the elastic-scattering hypothesis. To ascertain the discrimination of the χ^2 fit to background from reactions of the kind:

$$pp \rightarrow pp\pi^{o}$$
$$pp \rightarrow pp\pi^{o}\pi^{o} \qquad (3)$$

we proceeded as follows. We selected all four-pronged events belonging to the inclusive reaction:

$$pp \rightarrow p + \text{anything} \qquad (4)$$

where the final-state proton is slow in the laboratory. These events were converted into fake two-pronged events by ignoring all tracks except for the slow proton and the fastest positive track emerging from the main interaction point. These fake two-prongs were processed through our kinematic fitting programs and the fraction of events which fit the elastic hypothesis provided us with an estimate of the contamination of the elastic data from the sort of channels given in reaction (3). The uncertainty in this fitting procedure is reflected in the errors we assign to the two-prong cross sections. Errors on the $\geq$4-prong cross sections are mainly statistical.

Table II presents, at 405 GeV, results similar to those given in Table I. In Fig.1(b) we display the elastic scattering differential cross section for the higher energy data. The analysis proceeded in the same fashion as at 102 GeV. The larger error bars reflect the lower statistics as well as the poorer resolution for the two-pronged inelastic/elastic separation at 405 GeV.

Table III displays several calculated quantities of interest using the data presented in the previous tables. In Fig. 2 we combine our results with similar previous measurements at energies $\geq$ 50 GeV,[4] we note the following:

1. The average negative-particle multiplicity in inelastic pp collisions between 50 and 405 GeV rises approximately as $\ln s$. There is, however, a substantial scatter of the experimental points from a smooth

rise with s; this is true for all the inelastic data as well as for multiplicities excluding the two-pronged topology, thus suggesting the presence of interesting structure or additional systematic uncertainties in these experiments. The best fit linear dependence of $\langle n_- \rangle$ on $\ln s$ is $\langle n_- \rangle = -2.5 + 0.90 \ln s$. We do not quote errors on these parameters because of the poor quality of the fit (an additional quadratic term does not substantially improve the fit).

2. The f_2^- moment requires a $(\ln s)^2$ term in addition to a $\ln s$ term to obtain an acceptable χ^2 for its energy dependence:

$$f_2^- = (8.5 \pm 3.5) + (-3.8 \pm 1.3)\ln s + (0.43 \pm 0.12)(\ln s)^2$$

3. The errors on f_3^- are presently too large so as to discriminate between a linear or quadratic dependence on $\ln s$.

4. The value of $D/(\langle n \rangle -1)$ is approximately constant (~ 0.59) as predicted by Wroblewski. The ratios of the qth moments divided by the qth power of the mean multiplicity, i.e., $\langle n^2 \rangle / \langle n \rangle^q$ also appear to change slowly in this energy range (not shown). Taken together these results indicate that while exact KNO scaling does not hold in this energy regime, it may be approached asymptotically ($\sim$ as $1/\langle n \rangle$).[5]

We thank the members of the NAL neutrino laboratory for their aid in the taking of the exposures, and we thank our scanning and measuring personnel for their diligence.

References

1. J. Chapman et al., Phys. Rev. Letters 29, 1686 (1972).
2. The π^0 spectrum was obtained using γ-rays converting in the bubble chamber. See A. Seidl et al., Michigan/Rochester(preprint to be published), UMBC-7320, UR-457.
3. The real part of the forward elastic scattering amplitude is small and does not significantly affect eq. (2) V. Bartenev et al., Phys. Rev. Letters 29, 1755 (1972), and private communication from the authors.
4. The 50 GeV and 69 GeV data are from the French-Soviet Collaboration, Physics Letts. 42B, 519 (1972); the 205 GeV data are from G. Charlton et al., Phys. Rev. Letters 29, 515 (1972); the 303 GeV data are from the NAL-UCLA preprint, NAL 73/38, UCLA-1077.
5. Z. Koba, H. B. Nielsen and P. Olesen, Nuclear Phys. B40, 317 (1970). Also see the analyses given by P. Slattery, Phys. Rev. Letters 29, 1624 (1972), Phys. Rev. D7, 2073 (1973), and by A. Wroblewski in Lectures at XIII Cracow School of Theoretical Physics, 1973, to be published in Acta Physica Polonica. We stress the importance of the new data at 405 GeV , and the latest 303 GeV and 50 GeV results in reaching these conclusions.

Figure Captions

1. The differential cross-section for elastic scattering events at (a) 102 and (b) 405 GeV. The shaded area corresponds to the event losses at small t.
2. The negative particle multiplicity distribution moments and the expression $D/(\langle n\rangle - 1)$ as a function of the incident momentum. The curves are the result of logarithmic fits described in the text.

TABLE I

Topological Cross Sections at 102 GeV

Prong Number	Number Observed	Corrected[a] Number	Cross[b] Section (mb)
2	1266	Elastic 896	7.0 ± 0.4
		Inelastic 562	4.5 ± 0.4
4	1000	1012	7.9 ± 0.3
6	955	965	7.5 ± 0.3
8	745	743	5.8 ± 0.2
10	489	479	3.7 ± 0.2
12	218	209	1.6 ± 0.1
14	86	79	0.62 ± 0.07
16	29	27	0.21 ± 0.04
18	7	6	0.05 ± 0.02
20	2	2	0.016 ± 0.011
Total Inelastic		4084	31.9 ± 0.7
Total	4797	4980	38.9 ± 0.8

(a) See text.

(b) Density of hydrogen used in the calculation of cross sections is 0.0630 ± 0.0005 gm/cm^3.

TABLE II

Topological Cross Sections at 405 GeV

Prong Number	Number Observed	Corrected[a] Number	Cross[b] Section (mb)
2	600	Elastic 516 Inelastic 179	7.8 ± 0.7 2.7 ± 0.5
4	298	303	4.6 ± 0.3
6	331	336	5.1 ± 0.3
8	370	375	5.7 ± 0.3
10	312	313	4.7 ± 0.3
12	252	252	3.8 ± 0.2
14	190	187	2.8 ± 0.2
16	95	89	1.3 ± 0.1
18	66	63	0.95 ± 0.12
20	40	37	0.56 ± 0.09
22	23	21	0.32 ± 0.07
24	10	9	0.14 ± 0.05
26	3	2	0.030 ± 0.021
28	1	1	0.015 ± 0.015
30	2	2	0.030 ± 0.021
32	1	1	0.015 ± 0.015
Total Inelastic		2170	32.8 ± 1.0
Total	2594	2686	40.6 ± 1.2

(a) See text.

(b) Density of hydrogen used in the calculation of cross sections is 0.0630 ± 0.0005 gm/cm^3.

TABLE III

	102 GeV/c		405 GeV/c	
	All Charged	Negative Charge	All Charged	Negative Charge
$\langle n \rangle$	6.32 ±.07	2.16 ±.04	8.99 ±.14	3.50 ±.07
D	3.13 ±.04	1.56 ±.02	4.75 ±.09	2.37 ±.05
$\frac{\langle n \rangle}{D}$	2.02 ±.03	1.38 ±.03	1.89 ±.05	1.47 ±.04
$\frac{\langle (n-\langle n \rangle)^3 \rangle}{D^3}$ (a)	0.65 ±.04		0.75 ±.07	
$\frac{\langle (n-\langle n \rangle)^4 \rangle}{D^4}$ (a)	3.16 ±.13		3.62 ±.28	
f_2	3.45 ±.25	0.28 ±.07	13.5 ±.9	2.1 ±.2
f_3	3. ±1.	-0.50 ±.15	30. ±8.	0.1 ±.9
f_4	-34. ±7.	0.00 ±.34	30. ±100.	1. ±4.

(a) The skewness $(\langle (n-\langle n \rangle)^3 \rangle / D^3)$ and the kurtosis $(\langle (n-\langle n \rangle)^4 \rangle / D^4)$ are identical for the total and negative charged particle multiplicity distributions. D^2 is the variance of the multiplicity distribution, i.e., $D^2 = \langle (n - \langle n \rangle)^2 \rangle$.

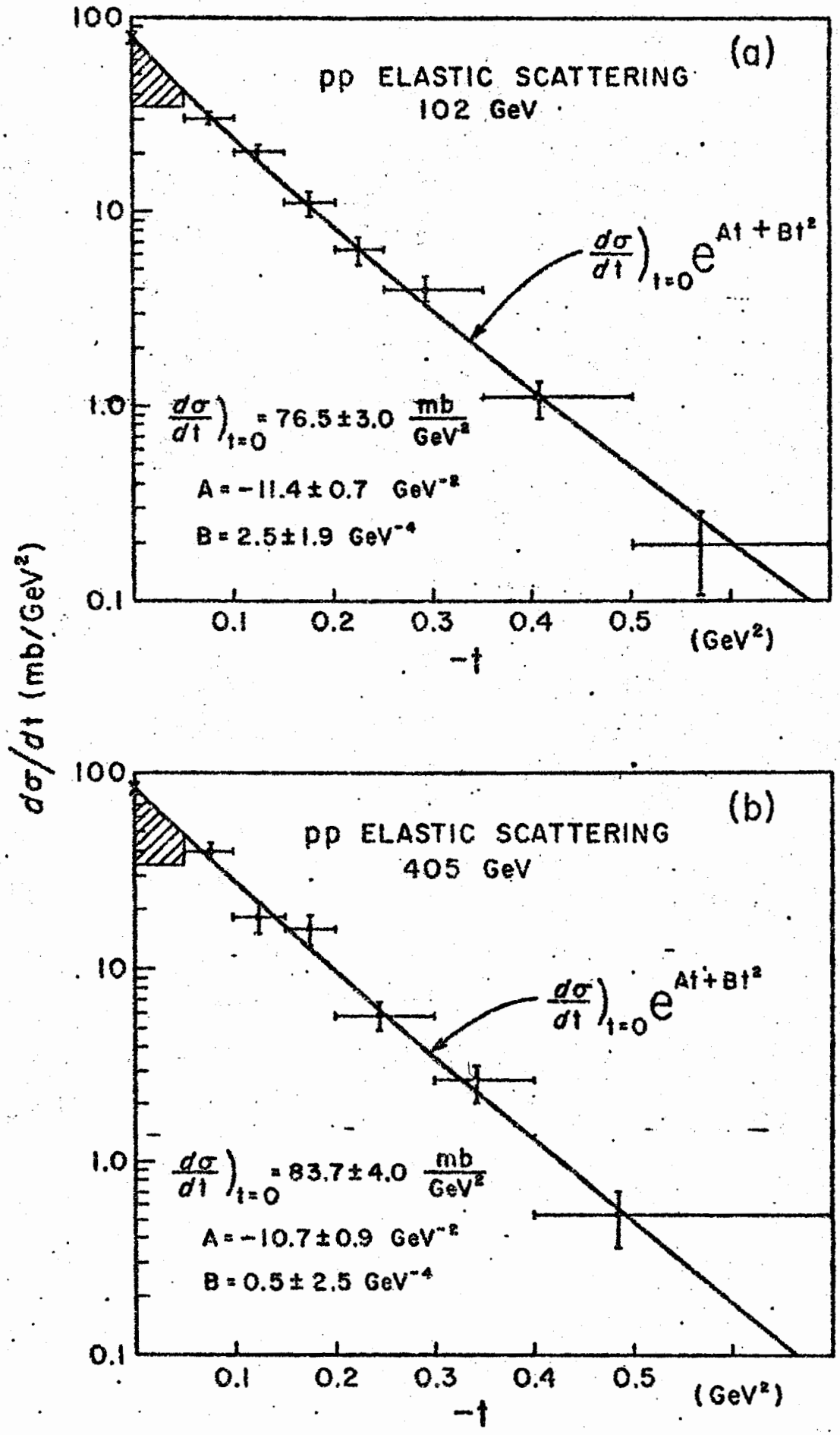
(a)
pp ELASTIC SCATTERING
102 GeV
$\left.\frac{d\sigma}{dt}\right)_{t=0} e^{At+Bt^2}$
$\left.\frac{d\sigma}{dt}\right)_{t=0} = 76.5 \pm 3.0 \ \frac{mb}{GeV^2}$
A = −11.4 ± 0.7 GeV⁻²
B = 2.5 ± 1.9 GeV⁻⁴
(b)
pp ELASTIC SCATTERING
405 GeV
$\left.\frac{d\sigma}{dt}\right)_{t=0} e^{At+Bt^2}$
$\left.\frac{d\sigma}{dt}\right)_{t=0} = 83.7 \pm 4.0 \ \frac{mb}{GeV^2}$
A = −10.7 ± 0.9 GeV⁻²
B = 0.5 ± 2.5 GeV⁻⁴
dσ/dt (mb/GeV²)
−t
(GeV²)
100
10
1.0
0.1
0.1
0.2
0.3
0.4
0.5

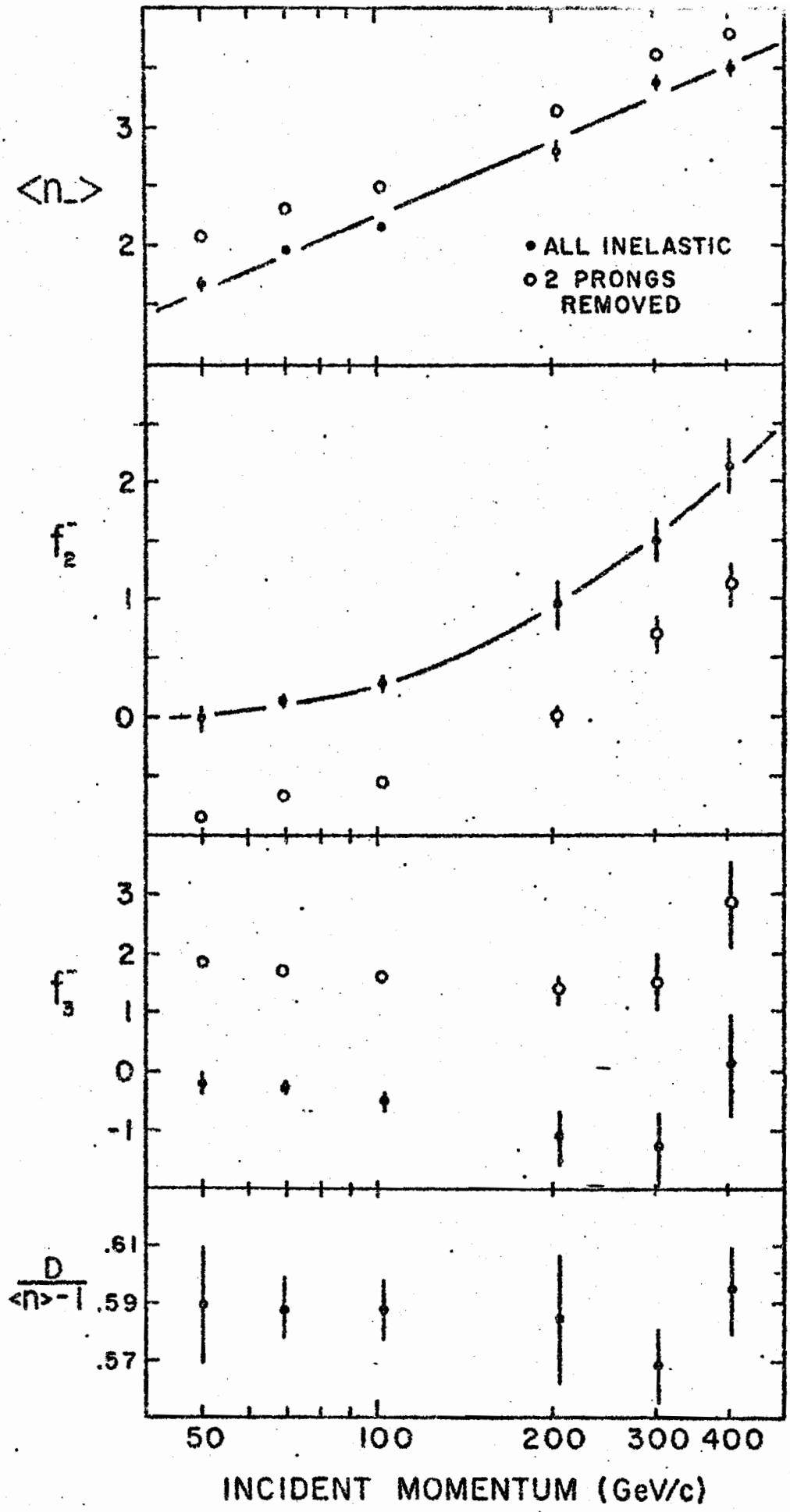
$\langle n_- \rangle$
3
2
• ALL INELASTIC
o 2 PRONGS REMOVED
f_2^-
2
1
0
f_3^-
3
2
1
0
-1
$\frac{D}{\langle n \rangle - 1}$
.61
.59
.57
50
100
200
300
400
INCIDENT MOMENTUM (GeV/c)